applied sciences

MDPI

Article

Numerical and Experimental Investigation of Flexural Properties and Damage Behavior of CFRTP/Al Laminates with Different Stacking Sequence

Shiyi Gao [1], Wenbin Hou [1,2], Jianing Xing [1] and Lin Sang [1,*]

[1] State Key Laboratory of Structural Analysis for Industrial Equipment, School of Automotive Engineering, Dalian University of Technology, Dalian 116024, China
[2] Ningbo Institute of Dalian University of Technology, Ningbo 315016, China
* Correspondence: sanglin@dlut.edu.cn

Abstract: Fiber Metal Laminates (FMLs) are hybrid materials that combine metal components with fiber-reinforced composites. The properties and failure modes of CArbon fiber Reinforced composites/Aluminum Laminates (CARALLs) composed of T700/PA6 unidirectional prepreg and 6061 aluminum alloy were studied using experimental and numerical simulation analysis. Through three-point bending experiments, the bending behavior of CARALLs with different composite/metal layer methods was examined. It was found that FMLs in the 2/1 patch form (one layer of aluminum and two layers of T700/PA6 unidirectional prepreg) show the highest bending modulus and strength compared with other stacking sequences. With the metal volume fraction increased, the bending properties of CARALLs decreased, suggesting the important role of the carbon fiber composite layer in the load-bearing capacity. Lastly, the Linde and Hashin failure criteria were employed to analyze the bending behavior and damage mechanism of CARALLs with different stacking sequences. The simulation results were in good agreement with the experimental results, which provides more insight into the prediction of the bending behavior of CARALLs hybrids.

Keywords: hybrid structures; numerical modeling; finite element analysis

check for updates

Citation: Gao, S.; Hou, W.; Xing, J.; Sang, L. Numerical and Experimental Investigation of Flexural Properties and Damage Behavior of CFRTP/Al Laminates with Different Stacking Sequence. *Appl. Sci.* **2023**, *13*, 1667. https://doi.org/10.3390/app13031667

Academic Editor: Maria Amélia Ramos Loja

Received: 30 December 2022
Revised: 20 January 2023
Accepted: 24 January 2023
Published: 28 January 2023

1. Introduction

At present, there is an increasing demand for high-performance materials in the industry, requiring them to have high mechanical properties as well as being lightweight. FMLs (Fiber Metal Laminates) are a modern hybrid material composed of metal alloys and fiber-reinforced polymers alternating between each other [1,2]. GLARE (Glass Fiber Reinforced Aluminum Laminates) is a successful example of FMLs, produced by laminating glass fiber reinforced prepreg and aluminum sheets, and has been commercialized. The FML materials have been continuously upgraded, including new metal alloys such as aluminum-magnesium alloys and titanium [3,4], and hybrids such as carbon fiber prepreg and carbon fiber woven fabric [5]. These laminates have been applied as aircraft components, such as the fuselage, wings, and other parts of aircraft. Additionally, with the optimization of the production process of materials and the reduction of production costs, FMLs are also being used in other industrial fields such as sporting goods and automotive engineering [6,7].

In recent years, numerous experiments have been conducted to analyze the dynamic and static mechanical properties of FMLs due to their advantages of lightweight, high-strength properties [8], corrosion resistance [7], favorable impact resistance [9,10], and damage tolerance [11,12]. The mechanical properties of GLARE have been extensively studied, and the lower modulus and strength of the glass fiber limited its application in load-bearing structures [13,14]. Consequently, CArbon fiber Reinforced composites/Aluminum Laminates (CARALLs), which are a combination of metal alloys and carbon fiber hybrids with higher modulus and strength, have become a focus of research [15]. In contrast with GLARE, CARALLs display lower density, higher specific strength, and superior stiffness [16,17]. However, due to the complex structure and hybrid materials of CARALLs, the mechanical properties and damage mechanisms are difficult to predict. Therefore, the damage behavior of FMLs under quasi-static conditions has attracted increasing attention [18,19]. Costanzo Bellini et al. studied the fracture patterns of FMLs under different loading conditions by using two different types of interfaces: structural adhesives or relying on the bonding ability of prepreg resins [20].

At present, most of the CFRP materials in CARALLs are thermosetting resin matrices; however, thermoplastic resin has superior properties such as higher damage tolerance, stronger impact resistance, and lower moisture absorption than the traditional thermoset resins. In addition, thermoplastic resins possess excellent recyclability. Jianing Xing developed MAPP/GF/Al fiber metal laminates, prepared with continuous glass fiber reinforced thermoplastic prepreg and maleic anhydride grafted polypropylene (MAPP) as the matrix resin. Compared with MAPP/GF control, the tensile and bending strength of 2/1 and 3/2 fiber metal laminates (FMLs) were maintained, while the modulus increased significantly [21]. Balakrishnan et al. also developed two different types of FRP-metal hybrid laminates and found that compared with epoxy resin polymer, PA6 had better adhesion to the steel surface, resulting in improved impact resistance of the thermoplastic-based FMLs [22].

Numerical simulation techniques have been utilized to simulate the quasi-static process of laminates, explore the specific damage forms inside FMLs, and analyze the energy absorption characteristics, providing an important reference value for the practical engineering application of laminates. To further understand the mechanical properties and failure mechanism of CARALLs under three-point bending, Hu et al. conducted experiments and numerical simulations. The results of the study shed light on the influence of stacked aluminum and carbon fiber hybrid layers on the mechanical properties of CARALL specimens [23]. Sellitto et al. conducted a study on the mechanical response of rectangular laminates under low-speed impact, featuring a numerical simulation method for analyzing the impact behavior of composite laminates [24].

The bending properties of FMLs have been studied by some researchers. Ostapiuk et al. conducted three-point bending tests to compare the bending and failure of GLARE and CARALLs under different aluminum thicknesses and fiber orientations [1]. Costanzo Bellini et al. studied the influence of superposition between the CFRP layer and aluminum plate and bonding interface on the mechanical behavior of CARALLs [20]. Although experimental methods are used to study the bending behavior and damage mechanism of CARALLs, finite element models display a more detailed stress-strain field with high designability. The simulation analysis could provide better insight into the failure of CARALLs. Furthermore, Hu et al. simulated the damage mechanism of CARALLs through Linde failure criteria. Hu H. et al. studied the application of Hashin criteria to CARALLs progressive failure analysis, but a single criterion alone has limited predictive capability [23]. However, previous studies did not consider complex layer methods, such as the stacking sequence of aluminum layers and carbon fiber-reinforced thermoplastic layers. Therefore, it is necessary to investigate the numerical simulation of the bending failure behavior of FMLs with proper failure criteria.

Typically, CARALL laminates, consisting of carbon fiber hybrids and metal layers, display outstanding mechanical properties that can be easily adjusted according to specific requirements by changing the fiber orientation, thickness, and number of layers [25]. When CARALLs are subjected to bending loading, the carbon fiber exhibits a brittle fracture while the polymeric matrix part displays toughness, forming a complex damage behavior and failure mode.

The development of carbon fiber-reinforced thermoplastic metal laminates is a novel hybrid material with lightweight and superior mechanical properties. However, the simulated models and failure criterion of CARALLs have been seldom reported. Therefore, the CARALLs with two stacking sequences were fabricated and the three-point bending experimental tests were conducted. Meanwhile, the failure behavior and damage mechanism of CARALLs were investigated by utilizing the Linde and Hashin failure criterion. The comparison between the two failure criteria and the bending behavior of this novel CARALL hybrid material are discussed.

2. Materials and Methods

2.1. Basic Materials Preparation

T700 carbon fiber /PA6 unidirectional prepregs (PA6/CF) were provided by the Ningbo Institute of Materials Technology and Engineering. Thermoplastic adhesive films were purchased from Foshan Duobang polymer materials Co., LTD. The aluminum alloy (6061-T6Al, 0.3, 0.6 mm) sheet was purchased from Shanghai Bixuan Metal Materials Co., LTD. The surface of the aluminum alloy was pre-treated by polishing. The performance parameters provided by aluminum alloy manufacturers are listed in Table 1. The material properties of fiber-reinforced thermoplastic prepregs were listed in Table 2.

Table 1. Material properties of 6061-T6 aluminum alloy.

Symbol	Property	Value
ρ	Density	2700 kg/m^3
E	Elastic modulus	71.6 GPa
ϑ	Possion's ratio	0.33
σ_s	Yield strength	252 MPa
σ_b	Tensile Strength	374 MPa
ε_f	Fracture strain	0.18

Table 2. Material properties of T700/PA carbon fiber unidirectional ply.

Symbol	Property	Value
ρ	Density	1000 kg/m^3
E_{11}	Longitudinal modulus	115 GPa
E_{22}	Transverse modulus	70 GPa
E_{33}	Elastic modulus	70 GPa
$\vartheta_{12}, \vartheta_{13}$	Possion's ratio	0.33
ϑ_{23}	Possion's ratio	0.45
G_{12}, G_{13}	Shear modulus	3700 MPa
G_{23}	Shear modulus	2000 MPa
X_t	Longitudinal tensile strength	2107 MPa
X_c	Longitudinal compressive strength	814 MPa
Y_t	Transverse tensile strength	35 MPa
Y_C	Transverse compressive strength	139.8 MPa
S	Shear strength	34.7 MPa
G_m	Matrix fracture energy	12.5 kJ/m^2
G_f	Fiber fracture energy	1 kJ/m^2

2.2. Fabrication of Fiber Metal Laminates

CARALLs were produced through a series of technological processes. To make the thermoplastic carbon fiber prepregs and aluminum alloys sheets combine to form FMLs, thermoplastic adhesive films were selected to assemble the two. The process was time-saving and high-efficiency without long-time curing of epoxy-based adhesives. The fabrication process of CARALLs included two stages. First, two layers of unidirectional thermoplastic prepreg were pressed into thin laminate (XLB-350 × 350, Qingdao Jinjiuzhou Rubber Machinery Co., LTD., Qingdao, China) along the direction of 0°. The forming temperature of PA6/CF was 250 °C with a compression pressure of 5MPa. The thermoplastic adhesive films were inserted between the aluminum sheet and the PA6/CF sheet.

Then, the aluminum alloy sheet and PA6/CF were assembled with adhesive films by hot pressing at 180 °C for 5 min. After cooling to a certain temperature, the formed fiber metal laminates (120 × 240 mm) were removed from the frame mold and cut into standard flexural specimens using CNC engraving. The manufacturing process is shown in Figure 1.

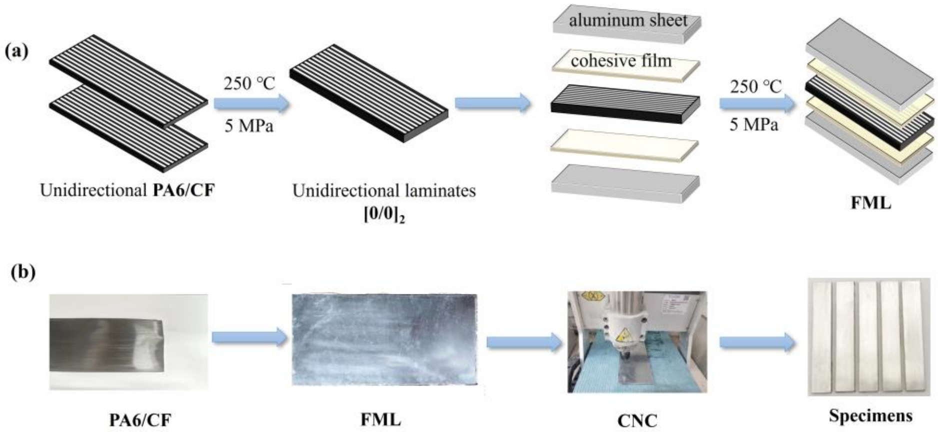

Figure 1. The manufacturing process of thermoplastic fiber metal hybrid laminates (**a**) The fabrication process of FMLs, (**b**) The production process of flexural specimens.

To understand the effect of stacking configurations on the flexural behavior of fiber metal laminates, two types of fiber metal laminates with different stacking configurations were designed. For type FMLs, the aluminum alloy sheets are set on the surface layer (top and bottom) and the fiber-reinforced thermoplastic laminates were placed between the aluminum alloy sheets. In contrast to the Type FMLs patch laminated structure, the hybrid laminates were on the external layer. The stack configuration details are shown in Figure 2. Furthermore, the influence of fiber volume fraction on the mechanical properties of thermoplastic fiber metal laminates was studied by designing 2/1 and 3/2 stacking structures. The stack details of sequences were shown in Table 3, and the code method was defined.

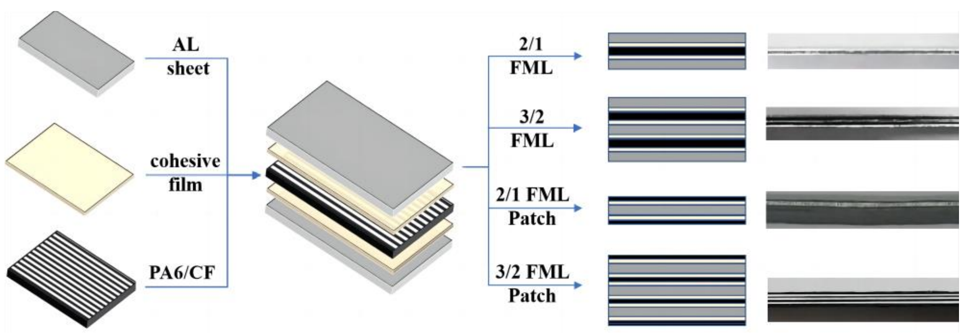

Figure 2. The detailed stacking configurations of thermoplastic fiber metal hybrid laminates.

Table 3. The abbreviation and stacking configuration of FMLs.

Structure	Stacking Configuration	Al Thickness (mm)	Mass (g)
2/1 FMLs	Al/[0/0]/Al	0.3	2.27
2/1 FMLs patch	0/Al/0	0.6	2.23
3/2 FMLs	Al/[0/0]/Al/[0/0]/Al	0.3	3.66
3/2 FMLs patch	0/Al/0/Al/0/AL/0	0.3	3.83

2.3. Three-Point Flexural Experiments

The bending performance of CARALLs was investigated by three-point bending experiments according to ASTM D7264. The specimens used for the tests were 78 mm in length, 13 mm in width, and a span of the support roll 60 mm. The tests were performed using a universal electronic testing machine (TSE105D, Shenzhen Wance Testing Machine Co., LTD.) at a displacement rate of 1 mm/min. To obtain reliable results, four parallel specimens were tested for each group and abnormal data were removed before calculating the average values. The loading head and the two supports were equipped with cylindrical contact surfaces with a radius of 5 mm, which were uniformly contacted across the entire width of the specimen. More detailed experimental parameters are shown in Figure 3.

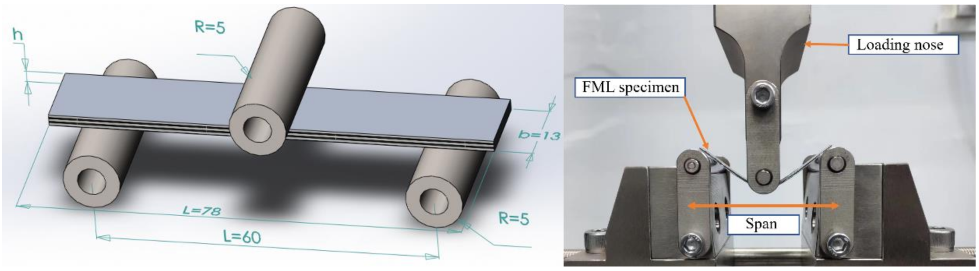

Figure 3. Details of three-point bending experiment and specimen size.

The flexural strength, maximum strain, and bending modulus of hybrid laminates were calculated as follows:

$$\sigma_f = \frac{3PL}{2bh^2} \tag{1}$$

$$\varepsilon_f = \frac{6\delta h}{L^2} \tag{2}$$

$$E_f = \frac{L^3 M}{4bh^3} \tag{3}$$

where P is the applied load, δ is the mid-span deflection, and M is the secant slope of the load-deflection curve.

3. Finite Element Modeling and Damage Criteria

3.1. Finite Element Model of Three-Point Bending of CARALL

To accurately model the behavior of the FMLs in finite element analysis, the radius of the loading nose and supports, and the size of FMLs were the same as those in the experiment. Face-to-face contact was adopted between the laminates, loading nose, and supports, and the normal contact attribute was set to hard contact, tangential contact attribute to penalty function, and friction coefficient to 0.15. The boundary condition of the supports was completely fixed, and symmetric constraints were set for the two surfaces of the laminates to avoid rigid body displacement. A reference point was set for the loading nose and all degrees of freedom except the loading direction were constrained. The loading displacement of the reference point was set, and the support reaction and displacement of the reference point were output to compare with the load-deflection curve obtained from testing. The aluminum alloy sheets, loading nose, and supports were modeled using C3D8I and R3D4 elements, respectively. The CFRP layer was modeled using the C3D8R element [26]. The material parameters used were consistent with those given in the chapter. Additionally, zero-thickness cohesive elements (COH3D8) were used to simulate the mechanical behavior between aluminum/CFRP layer and CFRP/CFRP layers [23,27]. The finite element model established according to the above material parameters and constraints is shown in Figure 4.

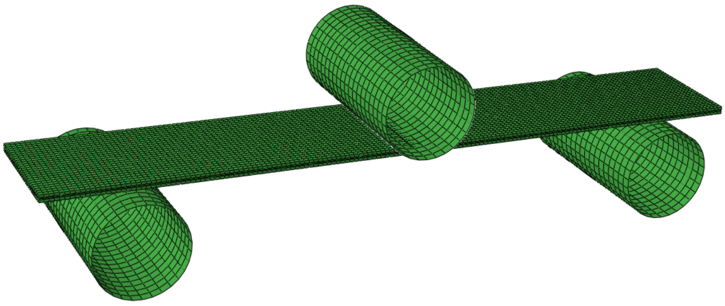

Figure 4. Finite element model of three-point bending test.

3.2. Damage Model for CARALL

3.2.1. Damage Model for Aluminum Sheets

The 6061-T6 aluminum alloy adopted an elastoplastic model. The linear elastic phase of aluminum alloy was modeled as an isotropic condition, defined by its elastic modulus and Poisson's ratio. Furthermore, the aluminum alloy utilized a ductility failure criterion [28] to judge its initial failure. This criterion suggest that plastic deformation occurs during the loading process of the material, leading to initiation, expansion, and aggregation of internal micropores and microcracks, which reduces the stiffness of the material and degrades its performance. The damage is assumed to occur when the equivalent plastic strain epsilon is a function of a three-axis stress and strain rate.

$$w_D = \int \frac{d\varepsilon^{pl}}{\varepsilon_D^{pl}(\eta, \dot{\varepsilon}^{pl})} = 1 \tag{4}$$

where $\eta = -p/q$, p is the compressive stress, q is the Von Mises equivalent stress, and w_D is the state variable that increases monotonically with the plastic deformation. Based on the continuum damage mechanics theory, the damage evolution process is as follows [29]:

$$\sigma = D^{\varepsilon l} : \left(\varepsilon - \bar{\varepsilon}^{pl}\right) \tag{5}$$

$$D^{\varepsilon l} = (1 - d) D_0^{\varepsilon l} \tag{6}$$

where $D_0^{\varepsilon l}$ is the initial elastic stiffness, $D^{\varepsilon l}$ is the stiffness after performance degradation, and ε^{pl} is the equivalent plastic strain at any time. The stiffness damage variable d changes from 0 to 1, representing the damage start to complete fracture.

3.2.2. Damage Model for CFRP Layers

The Linde criterion is a strain-based progressive damage model which suggests that material failure does not occur immediately after damage. Instead, the material still possesses some residual bearing capacity. This capacity is maintained through matrix failure, a non-fatal failure mode in which layers can withstand increasing loads even after the first layer is cracked. As the stress is redistributed, the damaged material is still able to withstand additional loads. The model takes into account different damage criteria for matrix and fiber failure [23]:

$$f_f = \sqrt{\frac{\varepsilon_{11}^{f,T}}{\varepsilon_{11}^{f,C}}(\varepsilon_{11})^2 + \left[\varepsilon_{11}^{f,T} - \frac{\left(\varepsilon_{11}^{f,T}\right)^2}{\varepsilon_{11}^{f,C}}\right]\varepsilon_{11}} > \varepsilon_{11}^{f,T} \tag{7}$$

$$f_m = \sqrt{\frac{\varepsilon_{22}^{f,T}}{\varepsilon_{22}^{f,C}}(\varepsilon_{22})^2 + \left[\varepsilon_{22}^{f,T} - \frac{\left(\varepsilon_{22}^{f,T}\right)^2}{\varepsilon_{22}^{f,C}}\right]\varepsilon_{22} + \left(\frac{\left(\varepsilon_{22}^{f,T}\right)}{\varepsilon_{12}^{f}}\right)^2 (\varepsilon_{12})^2} > \varepsilon_{22}^{f,T} \tag{8}$$

where f_f, f_m represent the failure modes of the fiber and matrix, and ε represents the strain of each side, where the superscript T represents the tensile direction and C represents the compression direction.

The Hashin criterion is a progressive damage model based on stress, similar to the Linde model. This model posits that the material still has some bearing capacity even after damage occurs, and considers the shear effect on fiber tensile failure. The Hashin criterion predicts four different failure modes: fiber tensile failure, fiber compression failure, matrix tensile failure, and collective compression failure. Therefore, it is more accurate to assess the degree of damage:

$$F_{ft} = \frac{\sigma_{11}^2}{X_T^2} + \alpha\left(\frac{\sigma_{12}^2 + \sigma_{13}^2}{S_{12}^2}\right)^2 = 1(\sigma_{11} \geq 0) \tag{9}$$

$$F_{fc} = \left(\frac{\sigma_{11}}{X_C}\right)^2 = 1, (\sigma_{11} < 0) \tag{10}$$

$$F_{mt} = \left(\frac{\sigma_{22} + \sigma_{33}}{Y_T^2}\right)^2 + \frac{\sigma_{12}^2 + \sigma_{13}^2}{S_{12}^2} + \frac{\sigma_{23}^2 + \sigma_{22}\sigma_{33}}{S_{23}^2} = 1, (\sigma_{22} + \sigma_{33} \geq 0) \tag{11}$$

$$F_{mc} = \left(\frac{\sigma_{22} + \sigma_{33}}{2S_{23}}\right)^2 + \left[\left(\frac{Y_C}{2S_{23}}\right)^2 - 1\right]\frac{\sigma_{22} + \sigma_{33}}{Y_C} + \frac{\sigma_{12}^2 + \sigma_{13}^2}{S_{12}^2} + \frac{\sigma_{23}^2 + \sigma_{22}\sigma_{33}}{S_{23}^2} = 1, (\sigma_{22} + \sigma_{33} < 0) \tag{12}$$

Similar to the Linde criterion, $F_{ft}, F_{fc}, F_{mt}, F_{mc}$ represent fiber tensile failure, fiber compression failure, matrix tensile failure, and matrix compression failure. σ represents the upward stress of each side, where the superscript T represents the tensile direction and C represents the compression direction. Y represents the strength in the direction of the fiber, X represents the strength in the direction of the matrix, and S represents the shear strength of each side.

Two different progressive damage models including the Linde criterion and Hashin criterion are compared in the current work. For the Linde criterion, the failure modes are classified into fiber failure and matrix failure. On the other hand, the Hashin criterion includes four failure modes including fiber tensile failure, fiber compression failure, matrix tensile failure, and matrix compression failure. However, the Hashin criterion does not always match the experimental results in the case of damage assessment, particularly for matrix compression failure. When moderate transverse compression impedes the interlaminar shear fracture of the specimen, the outcome using the Linde criterion might be different.

3.2.3. Damage Model for CFRP Layers

The interface between aluminum alloy and CFRP and the interface between two layers of CFRP may stratify. The cohesive zone model is used to simulate the failure behavior of the interface [30,31]. Material properties were shown in Table 4. The ABAQUS/Standard uncoupled traction separation constitutive model was selected to define the initial linear elastic behavior, as shown below:

$$\begin{bmatrix} t_n \\ t_s \\ t_t \end{bmatrix} = \begin{bmatrix} E_{nn} & 0 & 0 \\ 0 & E_{ss} & 0 \\ 0 & 0 & E_{tt} \end{bmatrix} \begin{bmatrix} \varepsilon_n \\ \varepsilon_s \\ \varepsilon_t \end{bmatrix} \tag{13}$$

where

$$\varepsilon_n = \frac{\delta_n}{T_0}, \varepsilon_s = \frac{\delta_s}{T_0}, \varepsilon_t = \frac{\delta_t}{T_0} \tag{14}$$

Table 4. Material properties of cohesive layers.

Symbol	Value
$E_{nn} = E_{ss} = E_{tt}$	100 GPa
t_n^0	5.37 MPa
t_s^0	36.62 MPa
t_t^0	36.62 MPa
G_n^c	0.23 kJ/m^2
G_s^c	0.48 kJ/m^2
κ	1.45
T_0	10^{-4} m

In addition, the secondary nominal stress criterion is used to judge the initial damage to the interface:

$$\left\{\frac{\langle t_n \rangle}{t_n^0}\right\}^2 + \left\{\frac{t_s}{t_s^0}\right\}^2 + \left\{\frac{t_t}{t_t^0}\right\}^2 = 1 \tag{15}$$

The damage evolution is based on the Benzeggagh-Kenane criterion of fracture energy:

$$G^C = G_n^C + \left(G_s^C - G_n^C\right)\left(\frac{G_S}{G_T}\right)^{\eta} \tag{16}$$

4. Result and Discussion

4.1. Influence of Stacked Structure on Flexural Properties

In this section, we discuss the result of the flexural experiment of two types of FMLs and the results of the simulation. These FMLs consisted of aluminum alloy sheets and unidirectional prepregs (as shown in Figure 2 and Table 2). The different modulus and strengths of aluminum alloy and carbon fiber-reinforced thermoplastic materials result in a distinct mechanical behavior.

Figure 5a,b illustrate the flexural stress-strain curves of FMLs with 2/1 stacking configurations. It can be seen that there is a significant difference. The curves are split into three main stages: elastic deformation, plastic deformation of the aluminum layer, and fiber breakage. In the first stage, the flexural load increases linearly and the specimen exhibits elastic deformation. At this stage, both the hybrid layer and the aluminum alloys layer are in the elastic stage and the specimens recover completely when the load is released. With continued loading, the hybrid layer remains in the elastic deformation stage, while the aluminum layer undergoes plastic deformation. In the third stage, the hybrid layer reaches the strain limit, then the fiber breaks and finally the load is reduced. There are no obvious cracks or fractures found in 2/1FMLs specimens during the bending process, indicating that the plastic deformation is mainly concentrated at the top and bottom of the aluminum alloy layer. However, the overall simulation curve is slightly higher than the test curve, which may be due to defects caused by the specimen-making process or excessive extrusion of the resin matrix in the molding.

The patch specimen 2/1 FMLs, as shown in Figure 5b, exhibits a different flexural failure behavior compared to the standard 2/1 FMLs. The flexural process can be divided into three stages. The flexural strength of the hybrid reaches its peak, with the patch-type 2/1 FMLs showing superior flexural strength to the standard 2/1 FMLs. In the following stage, the stress decreases rapidly due to the damage to the hybrid layer. Unidirectional prepreg strips placed in the form of patches on both sides of the metal layer cause the upper hybrid layer to experience compression loads and the lower hybrid layer to experience tensile loads during the compression process. Because the thermoplastic hybrid has a lower ductility than the metal layer, brittle fracture of the hybrid layer may occur in the second stage. In the third stage, the curve tends to become stable, suggesting the aluminum alloy layer becomes the main load-carrying. It can be seen from the simulation of patch-type 2/1 FMLs that Linde and Hashin criteria can accurately predict the flexural strength and modulus, as well as the failure behavior of the hybrid. This indicates that these criteria are reliable for the prediction of mechanical properties and exploration of mechanical behavior for the current 2/1 FMLs structure.

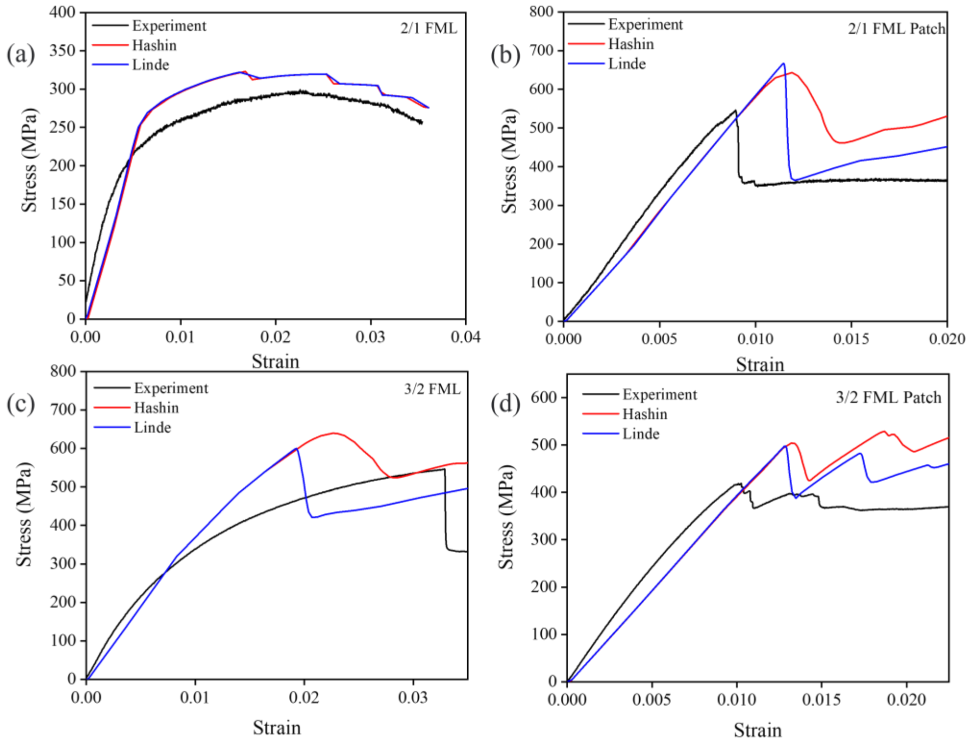

Figure 5. Flexural stress-strain curves of FMLs with different stack structures (**a**) 2/1 FMLs, (**b**) 3/2 FMLs patch, (**c**) 3/2 FMLs, (**d**) 3/2 FMLs patch.

The stress-strain curve of 3/2 FMLs specimens in the flexural experiment is shown in Figure 5c. Upon increasing the load, the stress curve initially rises linearly with an accompanying gradual increase in the bearing capacity of the specimens. After the linear phase, the specimen's mechanical behavior is manifested as an overall elastic mechanical characteristic. As the load continues to increase, the slope of the curve decreases noticeably, and the speed of stress-increase slows down until the peak load is reached. The sudden drop in load indicates that the tensile stress of the tensile part of the fiber has reached the failure stress, resulting in the failure of the hybrid material layer. Finally, with further strain increase, the stress gradually decreases, and the undamaged part of the fiber layer continues to bear the load.

The stress-strain curve of the flexural experiment of the 3/2 FMLs patch specimen is shown in Figure 5d. As the strain increased, the stress of the specimen increased linearly until the first failure strain point was reached, resulting in a sudden decrease in stress. After this initial drop, the stress of the specimen then increased again without further stability or decline. It is speculated that the first stress drop is related to the fracture of the first layer of carbon fibers and matrix failure. Due to the brittle failure mode of the carbon fiber layer, compression load causes the first layer to be damaged first, thereby reducing stress and increasing energy dissipation. This then allows the hybrid laminate to withstand higher strain levels. This is similar to the yield phase of metals, where the stress continues to increase until the material is destroyed, even though the rate of increase of stress slows down after the yield stress is reached. After the first stress drop, the load is redistributed to the following layers, allowing the laminates to bear the load again, and the stress to begin rising. This process is repeated with each subsequent layer of carbon fibers, resulting in a gradual decline in stress until complete failure. From this it can be seen that the 3/2 FMLs patch specimen is in a progressive damage mode, with the damage expanding at the interface layers and energy dissipation, allowing the specimen to withstand greater stress. The simulation results of 3/2 FMLs and 3/2 FMLs patch structure specimens show that the Linde criterion and Hashin criterion are still effective in predicting the mechanical properties and behaviors of more complex structures.

To validate the accuracy of the finite element simulation results, the bending modulus and bending strength of different laminated structures are compared and the results are shown in Figure 6. The experimental results and finite element results of the bending strength and bending modulus of FMLs with different layering structures show good agreement. It is observed that the material model adopted and the established finite element model can accurately simulate the bending performance of laminates. Furthermore, the finite element simulation results also demonstrated that the stack configuration has a substantial impact on the flexural property, and the trend was set by the test results with an error margin of 20%. It is also noticed that the patch-type specimens generally exhibit a higher modulus, whereas the 2/1 FMLs patch stack configuration displays an optimal overall mechanical property. Consequently, the validated finite element model is used to further analyze the stress distribution of each FML structure and the influence of the stack configuration on the flexural property of FMLs.

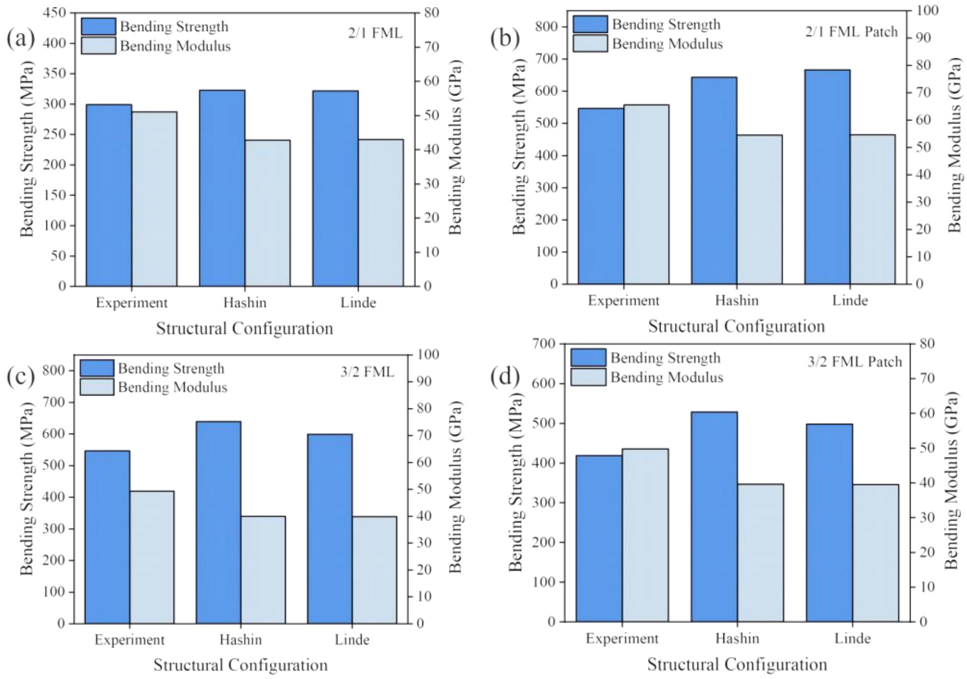

Figure 6. Bending modulus and strength of FMLs with different stack structures.

In this paper, a finite element model is established. It consists of an aluminum alloy layer of 0.6 mm, two thermoplastic prepreg layers, and three cohesive interface layers for the 2/1 FMLs structure, along with two aluminum alloy layers of 0.3 mm, two thermoplastic prepreg layers, and two cohesive interface layers for the 2/1 FMLs patch structure. These two types of stack configurations ensure that the metal and fiber volume fractions are the same. The longitudinal stress distribution contours at 2/1 FMLs failure time are shown in Figure 7a. During the three-point bending experiment, the top aluminum layer of the specimen of this structure is under compressive stress, while the bottom aluminum layer is under tensile stress. The upper half of the CFRP layer is compressed, while the lower half of the CFRP layer is stretched. As seen in the stress cloud diagram, the two simulation criteria have a similar trend in the simulation of longitudinal stress. The deflection at the time of failure of the Linde criterion is earlier than that of the Hashin criterion. The longitudinal stress distribution contours of the 2/1 FMLs patch structure are shown in Figure 7b. It can be seen that with the prepreg strips laid on the upper and lower sides of the aluminum alloy, the CFRP layer is further away from the neutral layer and the difference between tensile and compressive stress is more distinct compared to the 2/1 FMLs structure. The CFRP1 layer of the 2/1 FMLs patch is primarily under compressive stress, while the CFRP2 layer is primarily under tensile stress, which is quite different from 2/1 FMLs since the neutral layer is located between the CFRP layers in the 2/1 FMLs structure.

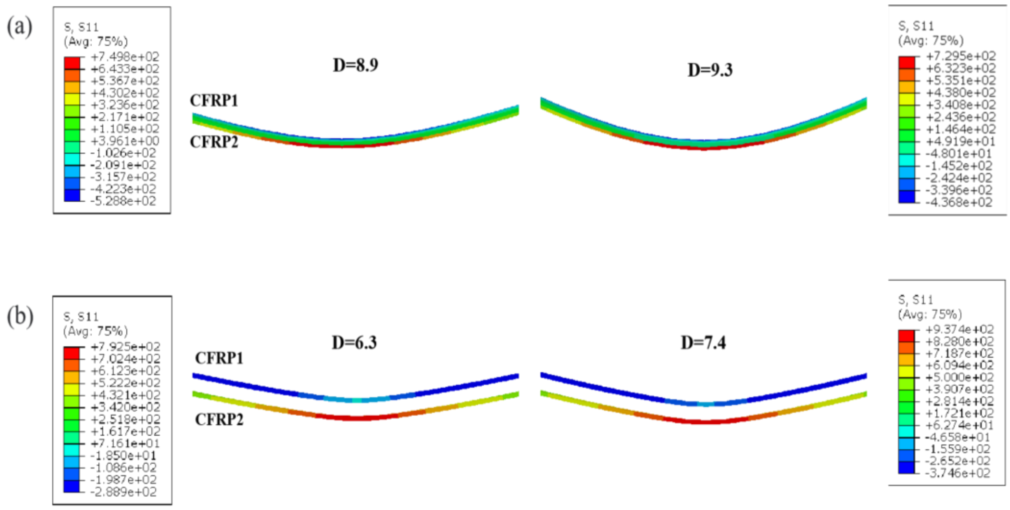

Figure 7. Longitudinal stress contours of 2/1 FMLs and 2/1 FMLs patch after failure (**a**) 2/1 FMLs, (**b**) 3/2 FMLs patch. (On the left is the Linde criterion and on the right is the Hashin criterion).

Similarly, in the finite element model established in this paper, the structure of 3/2 FMLs and 3/2 FMLs patch is, respectively, composed of 3 layers of aluminum alloy (0.3 mm), 4 layers of thermoplastic prepreg zone, 5 layers of the cohesive interface, as well as 3 layers of aluminum alloy (0.3 mm), 4 layers of thermoplastic prepreg zone, and 6 layers of cohesive interface. These two types of stack configurations ensure that the metal volume fraction and the fiber volume fraction are the same. Figure 8a shows the longitudinal stress distribution contours at the failure time of 3/2 FMLs. In a three-point flexural experiment, the specimen of this structure is similar to 2/1 FMLs in that the top aluminum layer is subjected to compressive stress and the bottom aluminum layer is subjected to tensile stress. Between each of the two aluminum layers, two layers of CFRP are inserted. Therefore, the upper half of the CFRP layer is subjected to compressive stress, while the lower half of the CFRP layer is subjected to tensile stress. As shown in the stress contours, it can be seen that the stress trend of the simulation of longitudinal stress is consistent between the two simulation criteria. Since one layer of CFRP layer is formed by the molding of two thermoplastic prepregs, except in the upper and lower aluminum alloy layers, the remaining structure and its failure mechanical behavior are very similar to that of 2/1 FMLs, which can also be seen from the stress-strain curve. Also, because the Linde criterion is relatively strict, the deflection at the time of failure is earlier than the Hashin criterion. The specimen contours of the 3/2 FMLs patch structure are shown in Figure 8b. It can be seen that when the prepreg belt is laid separately in the form of a patch instead of molding, the CFRP layer is further away from the neutral layer, and the difference between tensile stress and compressive stress of 3/2MLs, on the whole, is more distinct, especially for the lower part of CFRP layer. Due to the characteristics of the thermoplastic carbon fiber prepreg material, its tensile strength is much greater than the compression strength, and because the CFRP in the form of patch is not molded together, its synergy is worse than that of 3/2 FMLs, which can also be seen from the bending strength where 3/2 FMLs bending strength is greater than 3/2 FMLs patch.

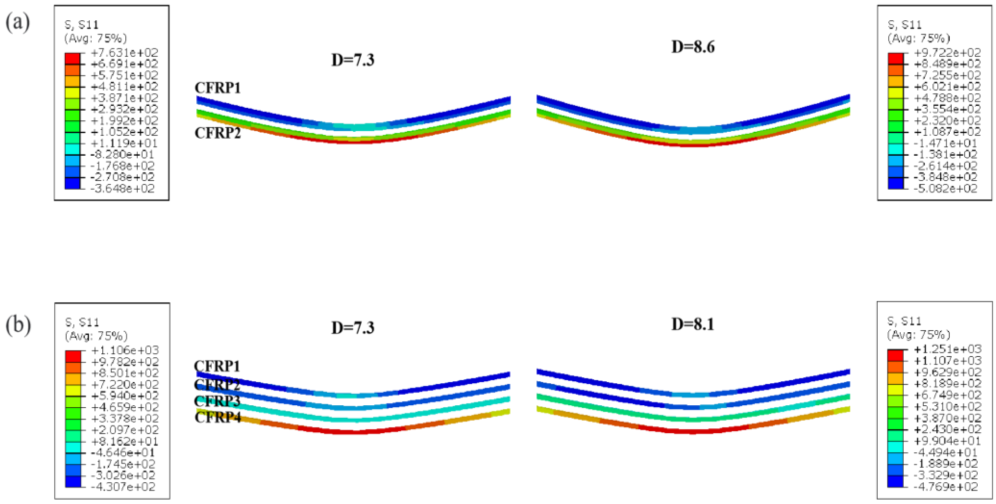

Figure 8. Longitudinal stress contours of 3/2 FMLs and 3/2 FMLs patch after failure (**a**) 3/2 FMLs, (**b**) 3/2 FMLs patch. (On the left is the Linde criterion and on the right is the Hashin criterion).

4.2. Failure Prediction and Damage Propagation Feature

In general, multi-material structures such as metal/fiber-reinforced hybrids may exhibit complex failure modes when subjected to load, such as metal fracture, buckling, fiber fracture, matrix cracking, and delamination. Depending on the stacking configuration and operational conditions, these failure modes can occur singly or in combination. Consequently, finite element analysis is necessary to accurately assess the failure of laminates. Both Linde and Hashin's models use two damage variables to describe hybrid material damage. The post-processing module's state that SDV1 represents the fiber damage variable, and SDV2 represents the matrix damage variable. The predicted damage of laminates is illustrated in Figures 9–12. For failure analysis, both three-dimensional constitutive models used in this paper can predict the progressive failure mode of hybrids in laminates. The failure mechanism layers are divided into two regions. The region above the neutral layer is the compression region, and the region below the neutral layer is the stretching region.

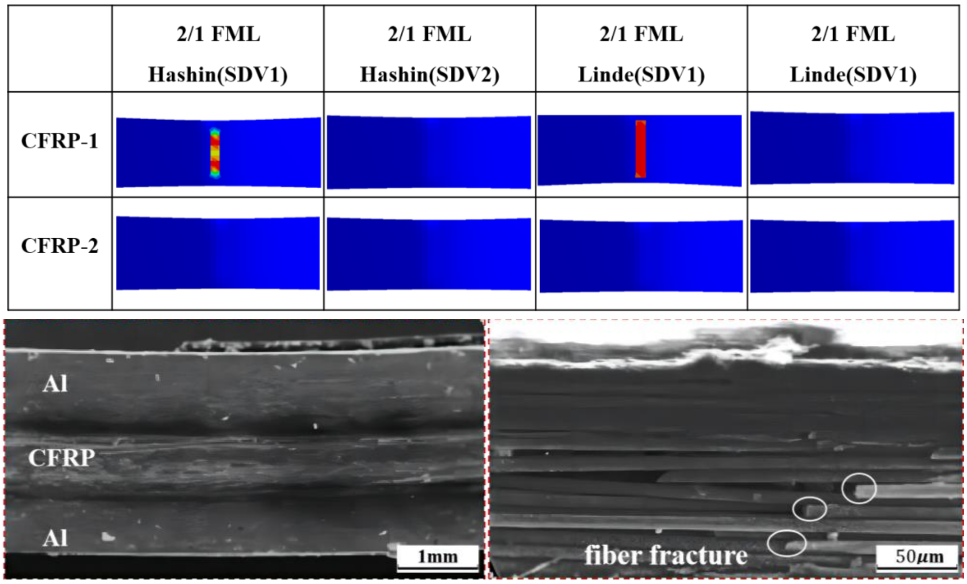

Figure 9. Damage of each CFRP layer in 2/1 FMLs.

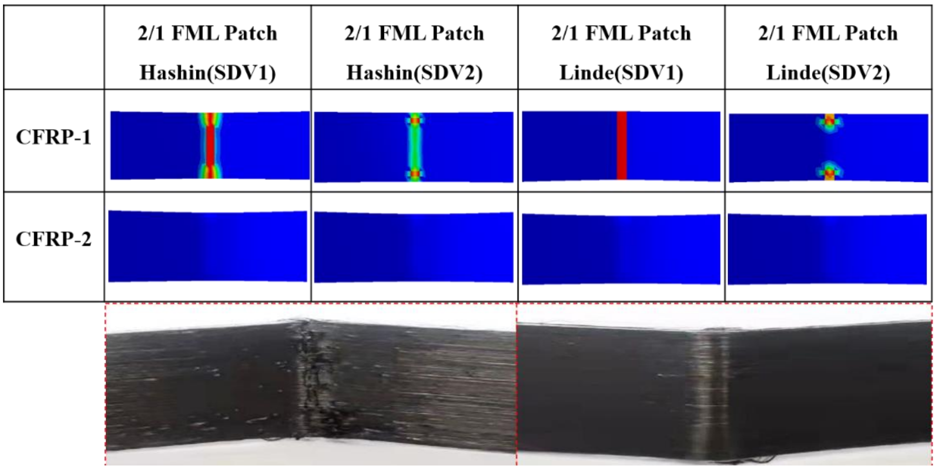

Figure 10. Damage of each CFRP layer in 2/1 FMLs patch.

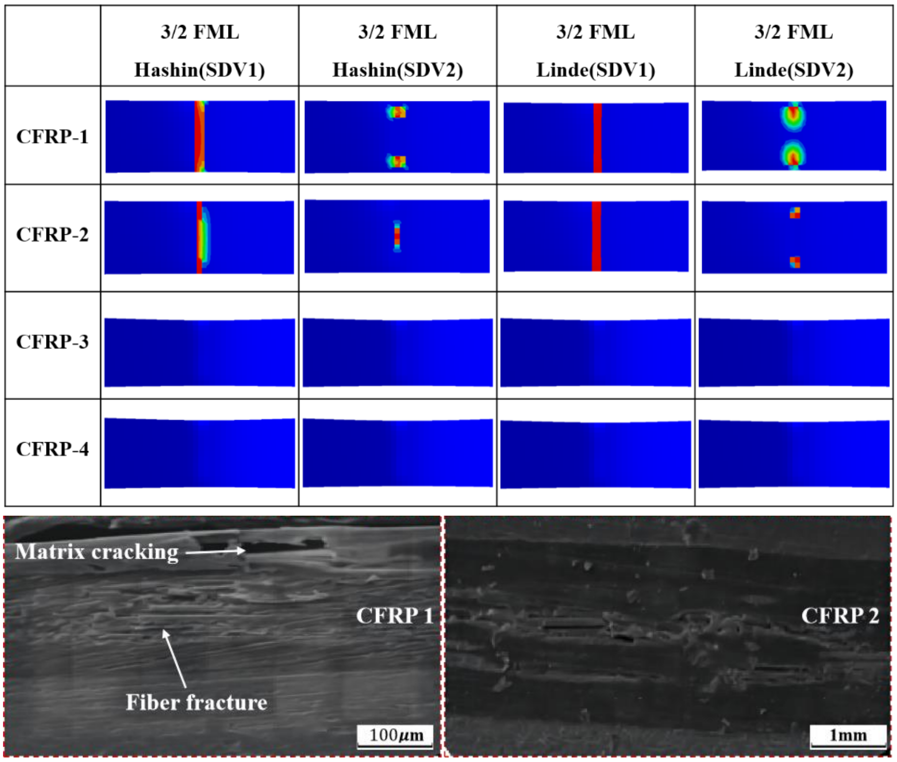

Figure 11. Damage of each CFRP layer in 3/2 FMLs.

As shown in Figure 9, for 2/1 FMLs, fiber breakage may begin at the 0° fiber layer above the neutral layer due to the relatively low compressive strength of carbon fiber than its tensile strength. The simulation results show that fiber fracture occurred in the CFRP1 layer above the neutral layer, while no damage is observed in the CFRP2 layer in the remaining tension area. The Linde criterion is stricter than the Hashin criterion, and thus causes more obvious fiber failure. Both criteria accurately simulate the matrix failure less result. The SEM images of microstructure of the side-section of FMLs specimens after three-point bending are provided in Figure 9. First, the hybrid Al and CFRP structures can be seen clearly. Except for local fiber fractures, no obvious damage is observed in the flexural specimen, which is consistent with the simulated results.

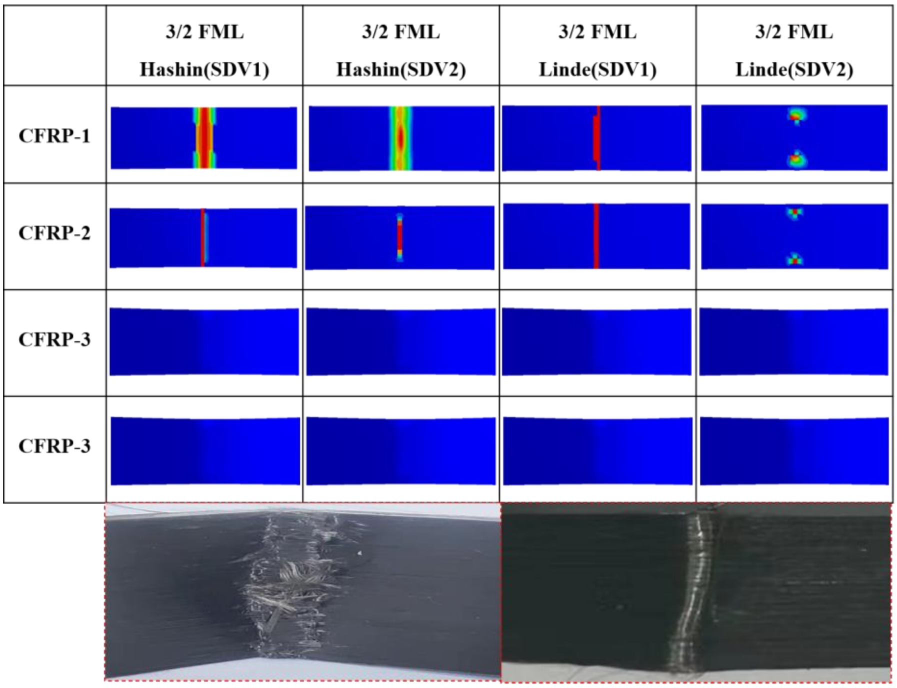

Figure 12. Damage of each CFRP layer in 3/2 FMLs patch.

As can be seen from Figure 10, since the 2/1 FMLs patch CFRP layer is far away from the neutral layer and directly contacts the loading head during the test, its fiber fracture failure and matrix failure are relatively obvious. Both simulation criteria show that the fiber fracture in the CFRP1 layer located in the compression zone is obvious, and the matrix fracture characteristics are typical. However, the CFRP2 layer below the neutral layer was not damaged. By comparing the real photos and the finite element analysis results, the damage condition is the same, and the failure prediction of the finite element model of 2/1 FMLs and 2/1 FMLs patch under a three-point bending condition is verified.

For 3/2 FMLs and 3/2 FMLs patch structures, the damage situation is more complex than usual. As seen in Fig. 11, the damage presented in the specimen of 3/2 FMLs structure is concentrated in the compression area at the upper part of the specimen. The fiber fracture failure and matrix fracture failure in the CFRP1 layer are predicted to be the same; however, the Hashin criterion suggests a different outcome for the matrix fracture failure in the CFRP2 layer. Linde criterion shows that the matrix failure is widespread around the matrix damage in the upper CFRP1 layer. Thus, the damage position predicted is in line with that of the CFRP1 layer, whereas the Hashin criterion predicts that the matrix failure in the CFRP2 layer is concentrated in the middle of the specimen, rather than at the edges. By SEM observations, matrix cracking and fiber fracture are observed in the CFRP-1 (upper) in 3/2 FMLs specimens, which is caused by the excessive bending displacement. But for the bottom part of 3/2 FMLs, minor damage exists in the CFRP-2 (bottom) layer. The damage of CFRP-1 and CFRP-2 layers in the experimental results are consistent with those by simulated analysis.

Regarding the specimens with the 3/2 FMLs patch structure, the CFRP layer is located further away from the neutral layer and directly contacts the loading head, resulting in more severe damage to the CFRP layer in the upper compression region of the specimen. The predictions of fiber fracture failure by the two criterion show consistency. Hashin criterion predicts fiber failure and matrix failure to be more serious than the Linde criterion in the CFRP1 layer. For the CFRP2 layer, the two criteria predict fiber failure in the same way, but in line with the 3/2 FMLs, the Linde criterion still predicts that the matrix failure is more spread around the matrix damage of the upper CFRP1 layer, while the Hashin criterion predicts that the matrix failure in the CFRP2 layer is more severe in the specimen that is far away from the two sides of the boundary line, and the CFRP layer in the tensile area is mostly undamaged. The comparison of physical figures further confirms that the finite element prediction results are generally consistent with the macroscopic representation.

5. Conclusions

In this paper, the three-point bending experiment and the numerical simulation analysis of Al/CFRP fiber metal laminates were conducted, and the relevant results were obtained. The failure behavior and damage mechanism of CARALLs were investigated by utilizing the Linde and Hashin failure criterion, and the feasibility of the failure criterion was discussed. The preliminary conclusions were as follows:

(1) The experimental results indicated that fiber fracture and matrix failure occurred in the CFRP layer above the neutral layer of the four structures of the laminates. Among the four stacking structures of laminates, the flexural modulus of FMLs of the patch-type was relatively higher because the CFRP layer directly contacted the loading head. Furthermore, the bending strength and modulus of laminate increase with the increase of fiber volume fraction, suggesting that the carbon fiber-reinforced hybrid layer played an important role in the bending property of laminates. The good consistency between the finite element simulation with the experimental results also demonstrated that the model is effective in predicting the performance of CARALLs.

(2) The macroscopic performance of the specimens and the finite element simulation both revealed that the CFRP layer in the compression region played an essential role in the bending property of the laminate. The main failure mechanism of the laminates was fiber compression fracture and matrix cracking of the CFRP layer. The tensile strength of fibers was much greater than the compression strength. The Linde and Hashin models implemented with the UMAT accurately predicted the failure behavior of the CARALLs.

(3) Some future work is still needed with the FE models involving failure criterial of hybrid materials being addressed. When analyzing the large deformations and damage evolution, implicit analysis is difficult to converge. More accurate material models in explicit analysis needs further exploring. Additionally, the effectiveness of the FE model proposed in this paper should be verified in future work.

Author Contributions: Methodology, J.X. and W.H.; software, S.G.; investigation, J.X. and S.G.; data curation, W.H. and S.G.; writing—original draft preparation, L.S. and S.G.; supervision, W.H.; project administration, L.S.; funding acquisition, L.S. and W.H. All authors have read and agreed to the published version of the manuscript.

Funding: This work was sponsored by the Fundamental Research Funds for the Central Universities (DUT21JC28) and the National Natural Science Foundation of China (No U21A20165, 52175216) and the Research Funds of the State Key Laboratory of Structural Analysis for Industrial Equipment (S22308).

Institutional Review Board Statement: Not applicable.

Informed Consent Statement: Not applicable.

Data Availability Statement: The data presented in this study are available on request from the corresponding author. The data are not publicly available due to on-going relevant study.

Conflicts of Interest: The authors declare no conflict of interest.

References

1. Ostapiuk, M.; Bienias, J.; Surowska, B. Analysis of the bending and failure of fiber metal laminates based on glass and carbon fibers. *Sci. Eng. Compos. Mater.* **2018**, *25*, 1095–1106. [CrossRef]
2. Rajkumar, G.R.; Krishna, M.; Narasimhamurthy, H.N.; Keshavmurthy, Y.C.; Nataraj, J.R. Investigation of Tensile and Bending behavior of Aluminum based hybrid fiber metal laminates. *Procedia Mater. Sci.* **2014**, *5*, 60–68. [CrossRef]
3. Nassir, N.A.; Birch, R.S.; Cantwell, W.J.; Sierra, D.R.; Edwardson, S.P.; Dearden, G.; Guan, Z.W. Experimental and numerical characterization of titanium -based fibre metal laminates. *Compos. Struct.* **2020**, *245*, 112398. [CrossRef]
4. Hu, Y.B.; Li, H.G.; Cai, L.; Zhu, J.P.; Pan, L.; Xu, J.; Tao, J. Preparation and properties of Fibre-Metal Laminates based on carbon fibre reinforced PMR polyimide. *Compos. Part B Eng.* **2015**, *69*, 587–591. [CrossRef]
5. Li, H.; Xu, Y.; Hua, X.; Liu, C.; Tao, J. Bending failure mechanism and flexural properties of GLARE laminates with different stacking sequences. *Compos. Struct.* **2018**, *187*, 354–363. [CrossRef]

6. Vermeeren, C. An historic overview of the development of fibre metal laminates. *Appl. Compos. Mater.* **2003**, *10*, 189–205. [CrossRef]
7. Sinmazcelik, T.; Avcu, E.; Bora, M.O.; Coban, O. A review: Fibre metal laminates, background, bonding types and applied test methods. *Mater. Des.* **2011**, *32*, 3671–3685. [CrossRef]
8. Kuhtz, M.; Buschner, N.; Henseler, T.; Hornig, A.; Klaerner, M.; Ullmann, M.; Jaeger, H.; Kroll, L.; Kawalla, R. An experimental study on the bending response of multi-layered fibre-metal-laminates. *J. Compos. Mater.* **2019**, *53*, 2579–2591. [CrossRef]
9. Yu, G.-C.; Wu, L.-Z.; Ma, L.; Xiong, J. Low velocity impact of carbon fiber aluminum laminates. *Compos. Struct.* **2015**, *119*, 757–766. [CrossRef]
10. Vieira, L.M.G.; Dobah, Y.; dos Santos, J.C.; Panzera, T.H.; Rubio, J.C.C.; Scarpa, F. Impact Properties of Novel Natural Fibre Metal Laminated Composite Materials. *Appl. Sci.* **2022**, *12*, 1869. [CrossRef]
11. Zhu, S.; Chai, G.B. Low-velocity impact response of fibre-metal laminates-Experimental and finite element analysis. *Compos. Sci. Technol.* **2012**, *72*, 1793–1802. [CrossRef]
12. Bienias, J.; Jakubczak, P.; Dadej, K. Low-velocity impact resistance of aluminium glass laminates-Experimental and numerical investigation. *Compos. Struct.* **2016**, *152*, 339–348. [CrossRef]
13. Yao, L.; Wang, C.; He, W.; Lu, S.; Xie, D. Influence of impactor shape on low-velocity impact behavior of fiber metal laminates combined numerical and experimental approaches. *Thin Walled Struct.* **2019**, *145*, 106399. [CrossRef]
14. Sharma, A.P.; Khan, S.H.; Parameswaran, V. Experimental and numerical investigation on the uni-axial tensile response and failure of fiber metal laminates. *Compos. Part B Eng.* **2017**, *125*, 259–274. [CrossRef]
15. Lin, Y.; Huang, Y.; Huang, T.; Liao, B.; Zhang, D.; Li, C. Characterization of progressive damage behaviour and failure mechanisms of carbon fibre reinforced aluminium laminates under three-point bending. *Thin. Walled Struct.* **2019**, *135*, 494–506. [CrossRef]
16. Dhaliwal, G.S.; Newaz, G.M. Compression after impact characteristics of carbon fiber reinforced aluminum laminates. *Compos. Struct.* **2017**, *160*, 1212–1224. [CrossRef]
17. Serna Moreno, M.C.; Romero Gutierrez, A.; Martinez Vicente, J.L. Different response under tension and compression of unidirectional carbon fibre laminates in a three-point bending test. *Compos. Struct.* **2016**, *136*, 706–711. [CrossRef]
18. Djabali, A.; Toubal, L.; Zitoune, R.; Rechak, S. An experimental investigation of the mechanical behavior and damage of thick laminated carbon/epoxy composite. *Compos. Struct.* **2018**, *184*, 178–190. [CrossRef]
19. Dhaliwal, G.S.; Newaz, G.M. Experimental and numerical investigation of flexural behavior of hat sectioned aluminum/carbon fiber reinforced mixed material composite beam. *Compos. Part B Eng.* **2020**, *182*, 107642. [CrossRef]
20. Bellini, C.; Di Cocco, V.; Iacoviello, F.; Sorrentino, L. Performance evaluation of CFRP/Al fibre metal laminates with different structural characteristics. *Compos. Struct.* **2019**, *225*, 111117. [CrossRef]
21. Xing, J.; Liu, S.; Gao, S.; Qu, S.; Sang, L. Mechanical performance of a novel glass fiber reinforced maleic anhydride grafted polypropylene composite and its thermoplastic-based fiber metal laminates. *Polym. Compos.* **2022**, *43*, 6180–6190. [CrossRef]
22. Balakrishnan, V.S.; Hart-Rawung, T.; Buhl, J.; Seidlitz, H.; Bambach, M. Impact and damage behaviour of FRP-metal hybrid laminates made by the reinforcement of glass fibers on 22MnB5 metal surface. *Compos. Sci. Technol.* **2020**, *187*, 107949. [CrossRef]
23. Hu, C.; Sang, L.; Jiang, K.; Xing, J.; Hou, W. Experimental and numerical characterization of flexural properties and failure behavior of CFRP/Al laminates. *Compos. Struct.* **2022**, *281*, 115036. [CrossRef]
24. Sellitto, A.; Saputo, S.; Di Caprio, F.; Riccio, A.; Russo, A.; Acanfora, V. Numerical-Experimental Correlation of Impact-Induced Damages in CFRP Laminates. *Appl. Sci.* **2019**, *9*, 2372. [CrossRef]
25. Sen, I.; Alderliesten, R.C.; Benedictus, R. Lay-up optimisation of fibre metal laminates based on fatigue crack propagation and residual strength. *Compos. Struct.* **2015**, *124*, 77–87. [CrossRef]
26. Hu, H.; Wei, Q.; Liu, B.; Liu, Y.; Hu, N.; Ma, Q.; Wang, C. Progressive Damage Behaviour Analysis and Comparison with 2D/3D Hashin Failure Models on Carbon Fibre-Reinforced Aluminium Laminates. *Polymers* **2022**, *14*, 2946. [CrossRef]
27. Rajabi, A.; Kadkhodayan, M.; Ghanei, S. An investigation into the flexural and drawing behaviors of GFRP-based fiber-metal laminate. *Mech. Adv. Mater. Struct.* **2018**, *25*, 805–812. [CrossRef]
28. Hooputra, H.; Gese, H.; Dell, H.; Werner, H. A comprehensive failure model for crashworthiness simulation of aluminium extrusions. *Int. J. Crashworthiness* **2004**, *9*, 449–463. [CrossRef]
29. Roux, E.; Shakoor, M.; Bernacki, M.; Bouchard, P.O. A new finite element approach for modelling ductile damage void nucleation and growth-analysis of loading path effect on damage mechanisms. *Model. Simul. Mater. Sci. Eng.* **2014**, *22*, 075001. [CrossRef]
30. De Cicco, D.; Taheri, F. Delamination Buckling and Crack Propagation Simulations in Fiber-Metal Laminates Using xFEM and Cohesive Elements. *Appl. Sci.* **2018**, *8*, 2440. [CrossRef]
31. Camanho, P.P.; Davila, C.G.; de Moura, M.F. Numerical simulation of mixed-mode progressive delamination in composite materials. *J. Compos. Mater.* **2003**, *37*, 1415–1438. [CrossRef]